Coherent Subnanosecond Switching of Perpendicular Magnetization by the Fieldlike Spin-Orbit Torque without an External Magnetic Field

William Legrand, Rajagopalan Ramaswamy, Rahul Mishra, and Hyunsoo Yang[*]

Department of Electrical and Computer Engineering, National University of Singapore, 117576 Singapore
(Received 18 February 2015; revised manuscript received 22 May 2015; published 18 June 2015)

We theoretically study the influence of a predominant fieldlike spin-orbit torque on the magnetization switching of small devices with a uniform magnetization. We show that for a certain range of ratios (0.23–0.55) of the Slonczewski torque to the fieldlike torque, it is possible to deterministically switch the magnetization without requiring any external assist field. A precise control of the pulse length is not necessary, but the pulse edge sharpness is critical. The proposed switching scheme is numerically verified by micromagnetic simulations to be effective in devices. Switching without any external assist field is of great interest for the application of spin-orbit torques to magnetic memories.

I. INTRODUCTION

The recent discovery of domain-wall propagation [1–3], current-induced switching [4–8], and high-frequency magnetization oscillations [9–11] induced by spin-orbit torque (SOT) in thin-film nanostructures has led to considerable research interest in the field of spintronics. It is notably expected that SOT allows high-speed, low-energy switching of magnetic devices which could benefit many technological applications, especially magnetic random-access memories. SOT switching of nanomagnets with either in-plane [6,8] or out-of-plane [5,7,12] magnetization has been investigated mostly in trilayered HM/FM/Ox structures, where a heavy metal (HM) is adjacent to a ferromagnetic (FM) layer capped by an oxide (Ox). In this configuration, an in-plane current can be applied to the trilayer to generate a perpendicular spin density from spin-orbit interaction, which is transferred to the FM and leads to switching. This perpendicular spin-density generation is currently attributed either to the spin Hall effect [2,7,13] in the HM layer or to the Rashba effect [1,5,14–17] at the FM/Ox interface, or both, and is still under debate. Regardless of the origin of the torque, the injected spin polarization is expected to be in-plane, so that compared to the previous configuration of spin-transfer torque with currents perpendicular to the plane [18], SOT allows faster, nonprecessional switching due to maximum initial torque efficiency.

However, as the injected spin polarization simply drives the magnetization in the plane, an external in-plane assist field has to be applied parallel to the current in order to achieve deterministic switching. The direction of switching is defined by the relative directions of both external field and applied current [5,7,19]. A recent study [20] has also underlined the essential role of the assist field in overcoming the Dzyaloshinskii-Moriya interaction (DMI) in large devices during the nonuniform switching process. It is possible to

obtain an external assist field in devices by engineering the magnetic stack, but this approach is hindered by disadvantages in terms of fabrication difficulties, efficiency, and stability. In fact, SOT switching without an external field has been recently demonstrated in specific structures with broken lateral inversion symmetry [21] or by engineering a tilted anisotropy [22]. Nevertheless, the ability to perform SOT switching without an assist field in standard magnetic stacks is of great interest for applications.

Current-induced SOT is often explained in terms of the fieldlike torque and the Slonczewski torque [1,7,23]. Recent experimental studies [24–28] found that the fieldlike torque can be much larger than the Slonczewski torque in some material combinations, and this fieldlike torque is also capable of switching the magnetization [29]. Here, we investigate the potential of SOT switching in the case where the fieldlike torque is predominant and combined with the Slonczewski torque. This study focuses on dynamic switching in small single-domain perpendicularly magnetized nanomagnets (typically, 50×50 nm^2 or less), which are of significant interest for applications. Our results show that for certain relative values of the Slonczewski and fieldlike torques, a deterministic switching of the magnetization can be achieved without an assist field. This switching is not sensitive to the pulse length but rather to the pulse rising time. Micromagnetic simulations are then performed to assess the suitability of this new approach for real devices, and to argue in favor of experimental feasibility.

SOT can be described [23] as the sum of the longitudinal (Slonczewski) torque $\boldsymbol{\tau}^{\parallel} \sim \mathbf{m} \times (\hat{\boldsymbol{\sigma}} \times \mathbf{m})$ and the transverse (fieldlike) torque $\boldsymbol{\tau}^{\perp} \sim \hat{\boldsymbol{\sigma}} \times \mathbf{m}$, where $\mathbf{m}$ denotes the direction of the magnetization vector and $\hat{\boldsymbol{\sigma}}$ collinear to $\hat{\mathbf{y}}$ is the in-plane polarization of the spin current, perpendicular to the current density $\mathbf{J} = J_e \hat{\mathbf{x}}$, as shown in Fig. 1(a). Thus, the evolution of the magnetization can be described by the Landau-Lifshitz-Gilbert equation, modified with the additional SOT contributions,

*eleyang@nus.edu.sg

064012-1

$$\frac{\partial \mathbf{m}}{\partial t} = -\gamma\mu_0 \mathbf{m} \times \mathbf{H}_{\text{eff}} + \alpha\mathbf{m} \times \frac{\partial \mathbf{m}}{\partial t} + \boldsymbol{\tau}^{\parallel} + \boldsymbol{\tau}^{\perp}, \quad (1)$$

where $\mathbf{m}$ is described in the polar coordinates (θ, φ), with the gyromagnetic ratio γ $(1.76 \times 10^7 \text{ Oe}^{-1}\text{ s}^{-1})$, the Gilbert damping constant α, and the effective field $\mathbf{H}_{\text{eff}} = H_{\text{ani}}(\cos\theta)\hat{\mathbf{z}} + \mathbf{H}_{\text{ext}}$ composed of both an effective anisotropy field and any external field applied along $\hat{\mathbf{x}}$, $\mathbf{H}_{\text{ext}} = H_x\hat{\mathbf{x}}$. We describe $\boldsymbol{\tau}^{\perp}$ and $\boldsymbol{\tau}^{\parallel}$ by their efficiencies $c^{\perp}$ and $c^{\parallel}$,

$$\boldsymbol{\tau}^{\perp} = \frac{\gamma\hbar c^{\perp}}{2|e|M_S t_{\text{FM}}} J_e(\hat{\boldsymbol{\sigma}} \times \mathbf{m}) \quad (2)$$

and

$$\boldsymbol{\tau}^{\parallel} = \frac{\gamma\hbar c^{\parallel}}{2|e|M_S t_{\text{FM}}} J_e[\mathbf{m} \times (\hat{\boldsymbol{\sigma}} \times \mathbf{m})], \quad (3)$$

where M_S and t_{FM} are the saturation magnetization and the thickness of the FM layer, respectively. Even if both of these torques do not necessarily arise from the spin Hall effect, we use this notation for comparison of efficiencies with spin Hall angles reported in the literature. Within this description, a positive value of $c^{\parallel}$ corresponds to a positive, equal value of the spin Hall angle [7]. It is also important to note that the Slonczewski torque does not necessarily compete with damping, and can contribute to or oppose damping proportionally to the cosine of the angle between $\hat{\boldsymbol{\sigma}}$ and $\mathbf{m}$, denoted by $\cos(\hat{\boldsymbol{\sigma}}, \mathbf{m})$ [30]. We can rescale the external field and the torques by the anisotropy effective field H_{ani} so that Eq. (1) is given in a convenient dimensionless form,

$$\frac{\partial \mathbf{m}}{\partial t'} = -\mathbf{m} \times [(\cos\theta)\hat{\mathbf{z}} + h_x\hat{\mathbf{x}}]$$
$$+ \alpha\mathbf{m} \times \frac{\partial \mathbf{m}}{\partial t'} - h^{\parallel}[\mathbf{m} \times (\mathbf{m} \times \hat{\boldsymbol{\sigma}})] - h^{\perp}(\mathbf{m} \times \hat{\boldsymbol{\sigma}}), \quad (4)$$

where $t' = \gamma\mu_0 H_{\text{ani}}t$ is a rescaled dimensionless time, $h_x = H_x/H_{\text{ani}}$, and $h^{\parallel,\perp} = H^{\parallel,\perp}/H_{\text{ani}} = (\hbar J_e c^{\parallel,\perp})/(2|e|\mu_0 M_S t_{\text{FM}}H_{\text{ani}})$ are the spin-orbit-torque effective fields.

As can be seen from Eq. (4), $\boldsymbol{\tau}^{\perp}$ generates a precession of $\mathbf{m}$ around its equivalent field $h^{\perp}\hat{\boldsymbol{\sigma}}$, and can then potentially lead to switching if the magnetization vector crosses the x-y plane. Previous theoretical works [31,32] modeled the current-induced SOT switching by only considering $\boldsymbol{\tau}^{\parallel}$, thus focusing on direct switching without precession. Other recent works [33] studied coherent switching in small nanomagnets with an in-plane assist field and a moderate $\boldsymbol{\tau}^{\perp}$ only. They underlined the oscillatory switching behavior depending on the length and intensity of the current pulse, similar to the behavior of orthogonal spin-torque (OST) devices [34,35]. To be able to deterministically switch the ferromagnet in this scheme, the current pulse needs to be precisely ended once the magnetization is reversed. On the contrary, a precise control of the pulse length is not necessary in our scheme, as discussed below.

To study the role of a dominant fieldlike torque, we solve Eq. (4) assuming a uniform magnetization in a small nanomagnet (for example, with dimensions of $w \times w = 50 \times 50 \text{ nm}^2$) and first discuss the trajectories qualitatively. To get a closer look into the expected behavior for real devices, we also give some illustrative numerical results using the magnetic parameters of CoFeB, such as $M_S = 1500 \text{ emu cm}^{-3}$, $\alpha = 0.01$, and $t_{\text{FM}} = 1.6$ nm. H_{ani} is set to 1000 Oe unless otherwise stated, which allows a stability factor up to $\Delta = \mu_0 M_S H_{\text{ani}}w^2 t_{\text{FM}}/2k_B T \sim 70$ at room temperature. We neglect all thermal contributions during switching. With these parameters, one can express $h^{\parallel,\perp} = c^{\parallel,\perp}(J_e/J_0)$ with a characteristic current density $J_0 = (2|e|\mu_0 M_S t_{\text{FM}}H_{\text{ani}})/\hbar = 7.28 \times 10^7 \text{ A cm}^{-2}$.

II. QUASISTATIC REGIME

We first briefly recall the switching scenario under an assist field, when $\boldsymbol{\tau}^{\perp}$ is not taken into account or is negligible [31,36]. The anisotropy allows two equilibrium positions for the magnetization, an up ($\mathbf{m}$ pointing close to $+\hat{\mathbf{z}}$) and a down ($\mathbf{m}$ pointing close to $-\hat{\mathbf{z}}$) equilibrium, both slightly tilted away from the z axis because of the in-plane external assist field. Let us consider that the initial position of $\mathbf{m}$ is at the up equilibrium position. As the current gradually increases, the up and down stable equilibria are progressively driven closer to $+\hat{\mathbf{x}}$ and $-\hat{\mathbf{x}}$, respectively, while staying in the x-z plane. When the critical (positive) value of the current is reached, the up position is suppressed and $\mathbf{m}$ switches to an intermediate equilibrium, away from the x-z plane and close to $\hat{\boldsymbol{\sigma}}$ [31]. The assist field is actually not required to suppress the up equilibrium. Without an external field, the critical value of the torque to suppress both up and down equilibria is identical, $h^{\parallel}_{u,d} = 0.5$ [36]. The role of the assist field is to induce asymmetry between the ranges of $h^{\parallel}$ for which the up and down equilibria exist (with $h^{\parallel}_d > 0.5$ and $h^{\parallel}_u < 0.5$), so that the down position is still a stable equilibrium when the up state is no longer an equilibrium. After the pulse falling edge, $\mathbf{m}$ eventually relaxes to the down position.

To achieve the opposite switching event (i.e., from down to up) through a symmetric process, either an opposite value of the assist field or an opposite value of the current needs to be applied. This scenario relies on the quasistatic evolution of $\mathbf{m}$ and then describes accurately the most-studied case of SOT quasistatic switching, using either a direct current or a current pulse of rising time much longer than the characteristic time of precession ($t' = 2\pi$, that is corresponding to $t \approx 0.36$ ns in our case). In this work, the current is modeled as a trapezoidal pulse with equal rising and falling time, t_{rise}. When the corresponding value $t'_{\text{rise}} = \gamma\mu_0 H_{\text{ani}}t_{\text{rise}}$ is much greater than 2π, switching occurs as described above, following quasistatic evolution.
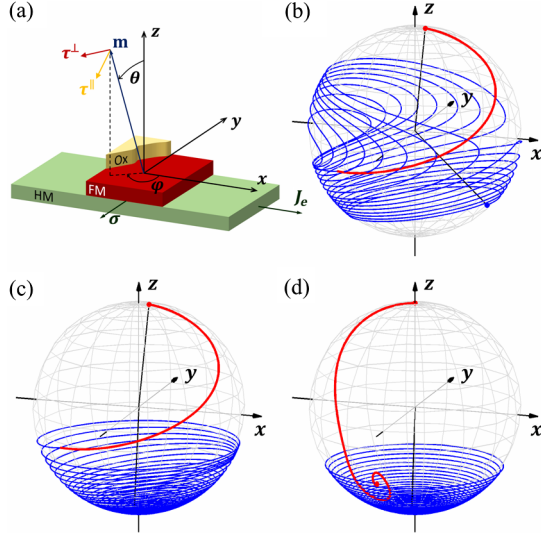
FIG. 1. (a) A sectional view of the trilayered system and directions of the different torques. (b), (c) Field-assisted trajectory of the magnetization with $t'_{rise} = 40\pi$, $h_x = 0.1$, $h^{\parallel} = 0.45$, and $h^{\perp} = 0$ (b), $h^{\perp} = 0.005$ (c). (d) Switching trajectory without an assist field ($h_x = 0$) with $t'_{rise} = 0, h^{\parallel} = 0.2$, and $h^{\perp} = 0.8$. The red (blue) curve represents the dynamics of **m** under a current pulse (for the subsequent relaxation), and the red (blue) dot indicates the original direction of **m** (direction after applying the pulse and relaxation). Relaxation within only 20 ns is shown for clarity.

The scenario of switching due to a slowly varying current pulse is exemplified in Fig. 1(b), which shows the switching trajectory for $h^{\parallel} = 0.45$, $h_x = 0.1$, and $t'_{rise} = 40\pi \gg 2\pi$. The switching trajectory to the intermediate equilibrium is represented by the red curve, and the subsequent relaxation by the blue curve. Assuming a macrospin behavior in the case of a Slonczewski torque only, the relaxation event disturbs the switching process. As revealed by numerical simulations [31] and as can be understood from the many precessions during the relaxation in Fig. 1(b), the final position between up and down is extremely sensitive to the values of α and $h^{\parallel}$.

Such an unpredictable relaxation is due to the hysteretic behavior of the transition to the intermediate position [36], that involves dynamics during the relaxation, even in the case of a slow evolution of the applied current. With the parameters of Fig. 1(b), the minimum value of $h^{\parallel}$ needed for the intermediate position to be stable in our simulations, which we define as $h^{\parallel}_i \approx 0.325$, is significantly lower than $h^{\parallel}_u \approx 0.43$ (one can derive the same values from Ref. [36]). After switching to the intermediate position when $h^{\parallel} > h^{\parallel}_u$, **m** is destabilized only when $h^{\parallel} < h^{\parallel}_i$, which happens during the falling edge of the pulse. At this time, both up and down equilibria are stable again and located far from $\hat{\sigma}$, so that **m** can relax to either one through a large dynamic precession covering both $z < 0$ and $z > 0$ half-spheres [Fig. 1(b)]. The unpredictability of the dynamics to the final position is amplified even more by the low value of α, as the

precession amplitude remains large after the current falling edge so that many oscillations occur, resulting in non-deterministic switching.

Considering the above hysteretic behavior of the transition to the intermediate position brings two conclusions. (i) It explains clearly why a higher α [31,33] that damps the oscillations during relaxation from the intermediate state (and also destabilizes the intermediate equilibrium earlier) enables the deterministic field-assisted switching. By increasing α to 0.04 (not shown) in the situation of Fig. 1(b), even though switching occurs through the intermediate equilibrium, the relaxation trajectory is damped enough to remain in the $z < 0$ half-sphere and switching is deterministic. (ii) As the intermediate position is shifted and modified by the in-plane assist field, h_x also contributes to the destabilization of the intermediate equilibrium, and one can refer to Ref. [36] to find the minimum value of α, so that $h^{\parallel}_u < h^{\parallel}_i$ at a given h_x. When α is greater than this minimum, the intermediate position is unstable when the up equilibrium is suppressed, and **m** directly switches to the down equilibrium position ($h^{\parallel} < h^{\parallel}_d$), ensuring deterministic switching. For $h_x \approx 0.15$ or higher, the intermediate equilibrium is unstable at $h^{\parallel}_u$, regardless of α, and switching directly proceeds to the final $-\hat{z}$ direction (not shown).

We extend the study of quasistatic switching to the influence of the fieldlike torque as well, and find that the transverse field from $\boldsymbol{\tau}^{\perp}$ allows deterministic quasistatic switching, even with a low α. As the intermediate position is shifted and modified by the fieldlike torque as well, it is destabilized much earlier and the relaxation proceeds only in the $z < 0$ half-sphere. Keeping the parameters of Fig. 1(b) and $\alpha = 0.01$ but adding a small fieldlike torque ($h^{\perp} = 0.005$), switching is found to be deterministic, as shown in Fig. 1(c). These results indicate that it is necessary to consider the dynamics and the fieldlike term, as they may have a critical influence on the SOT switching.

III. DYNAMIC REGIME

A. Switching mechanism

The role of $\boldsymbol{\tau}^{\perp}$ can be much more significant than enhancing the field-assisted switching, as we show that a predominant fieldlike torque enables switching without any assist field. Figure 1(d) shows one example of switching without an assist field ($h_x = 0$), in the case of a dominant fieldlike torque with $h^{\parallel} = 0.2$ and $h^{\perp} = 0.8$, corresponding to $c^{\parallel}/c^{\perp} = 0.25$. The rising time t_{rise} is assumed as infinitely small and, thus, negligible compared to the characteristic period of precession of the system, so that the dynamics of **m** dominates switching. As can be seen from the red part of the trajectory, **m** precesses around $\hat{\sigma}$ to cross the x-y plane at $t' \approx 0.81\pi$ or $t \approx 145$ ps, which is about half of the characteristic precession time, and directly stabilizes at the down equilibrium position (after $t' \approx 5.6\pi$

or $t \approx 1$ ns). The blue part of the trajectory corresponds to the final relaxation after the falling edge of the pulse and indicates that **m** has finally switched.

In order to understand the switching mechanism, first consider the case of a sole fieldlike torque. Due to the sharp increase of the current pulse, **m** is still parallel to $\hat{\mathbf{z}}$ when the maximum level of the current pulse is reached, inducing a large lag between **m** and the up equilibrium displaced by the spin-orbit torques. This lag actually raises the energy of the system relative to the new energy minima, corresponding to the displaced up and down equilibrium positions, and any dissipation would need some time to occur. Moreover, because of the fieldlike-torque effective field being a transverse field, the up- and down-equilibrium positions are tilted away from the x-z plane toward $\hat{\boldsymbol{\sigma}}$. For a sufficiently high value of the current, the trajectory of constant energy starting from $+\hat{\mathbf{z}}$ and winding around the displaced up equilibrium merges with the symmetric orbit winding around the displaced down equilibrium. This creates a large trajectory of precession which conjugates the two up and down states by winding around them [Fig. 2(a)]. The critical $h^{\perp}$ value ($h^{\perp} = 0.5$) to observe this merging corresponds to when the homoclinic orbits of the system (which start from $\hat{\boldsymbol{\sigma}}$) reach $\pm\hat{\mathbf{z}}$. This occurs when $E(\pm\hat{\mathbf{z}}) = E(\hat{\boldsymbol{\sigma}})$, with the energy density of the system derived from the anisotropy and fieldlike torque effective fields, $E(\mathbf{m}) = -\mu_0 M_S H_{\text{ani}}[(\mathbf{m} \cdot \hat{\mathbf{z}})^2/2 + h^{\perp}(\mathbf{m} \cdot \hat{\boldsymbol{\sigma}})]$.

Such a precessional motion from the fieldlike spin-orbit-torque scenario is similar to the well-known field-pulse-induced switching [37]. The precession of **m** is progressively damped while the current pulse is maintained [Fig. 2(b)], until **m** finally falls into one hemisphere, leading to either switching or nonswitching in an unpredictable manner. By adjusting the length of the pulse, the current can be stopped at the time when **m** reaches the down equilibrium, ensuring that switching is achieved. However, such a switching scheme may not be practical for applications, because the switching pulse length needs to be modified according to any variations of the FM layer's magnetic properties, field efficiency, and current. It is also found that, due to the Gilbert damping of the precession, switching back can be prevented after switching from one equilibrium to another, so that a reliable, deterministic switching of the magnetization can be obtained for any pulse length longer than the required switching time [37]. However, as this regime is damping dominated, the shorter switching times are not reachable. The well-balanced combination of the Slonczewski and fieldlike torques addresses these limitations and leads to the fast and deterministic switching observed in Fig. 1(d).

By choosing $c^{\parallel}/c^{\perp}$ significantly lower than unity but not negligible, the Slonczewski torque has a limited but crucial influence on switching, as we discuss below. Different cases with increasing the Slonczewski torque are shown in Figs. 2(c)–2(f). As the fieldlike torque dominates, **m**
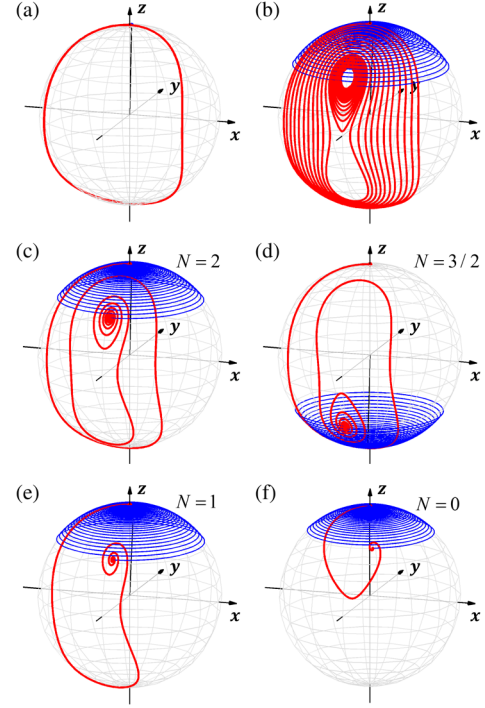

FIG. 2. (a) Trajectory obtained in the event of conservation of the energy with $\alpha = 0$ and $t_{\text{rise}} = 0$, that is, the isoenergetic orbit. Relaxation is not shown. (b) Dissipative trajectory obtained with $\alpha = 0.01$. Under the application of currents, **m** finally falls into one hemisphere and relaxes to $+\hat{\mathbf{z}}$ in this case, but the final state, up or down, is not controllable. For both (a) and (b), $h^{\parallel} = 0$ and $h^{\perp} = 0.8$. (c)–(f) Trajectories for various values of $h^{\parallel}$ and $h^{\perp}$: (c) $h^{\parallel} = 0.04$ and $h^{\perp} = 0.8$, (d) $h^{\parallel} = 0.05$ and $h^{\perp} = 0.8$, (e) $h^{\parallel} = 0.1$ and $h^{\perp} = 0.8$, and (f) $h^{\parallel} = 0.3$ and $h^{\perp} = 0.6$. The precession order N is indicated in each case. For (b)–(f), pulse length is 20 ns with no rising time, and relaxation within only 20 ns is shown. In each plot, the red (blue) curve represents the dynamics of **m** under the current pulse (for the subsequent relaxation).

precesses around $\hat{\boldsymbol{\sigma}}$ and the two equilibrium positions up and down are shifted toward $\hat{\boldsymbol{\sigma}}$, which is similar to the previous case of the sole fieldlike torque shown in Fig. 2(b). Under the application of currents, the up- and down-equilibrium positions are also slightly shifted along the x axis by the Slonczewski torque, as it is noticeable in Figs. 2(c)–2(f). However, the nature of the trajectories remains unchanged, and **m** still crosses the x-y plane at some point. Along the trajectory of **m** precessing around $\hat{\boldsymbol{\sigma}}$, which is located on the half-sphere with $y < 0$ in all cases, the Slonczewski torque always generates a positive damping as $\cos(\hat{\boldsymbol{\sigma}}, \mathbf{m})$ has a positive sign. In analogy with the case of the field-pulse-induced switching [37], it is natural to define a precession order N which is a half-integer counting the number of rotations of **m** around $\hat{\boldsymbol{\sigma}}$. By increasing the Slonczewski-torque efficiency, the effective damping is consequently enhanced. As a result, the additional energy obtained from the lag is dissipated faster, limiting N to lower values for larger $c^{\parallel}$ [see Figs. 2(b)–2(f)]. In the

particular case of Fig. 2(f), the damping on the trajectory is so strong that **m** never crosses the *x-y* plane. Back to the example of Fig. 1(d), where $c^{\parallel}/c^{\perp} = 0.25$, we now understand that the Slonczewski torque is strong enough to efficiently damp the precession arising from the fieldlike torque, so that **m** is rapidly stabilized [38] at the down equilibrium for the remaining part of the pulse, resulting in $N = 1/2$. As there is no assist field, the precession during relaxation cannot assist **m** to again cross the *x-y* plane backwards, and **m** eventually relaxes to $-\hat{\mathbf{z}}$ after the pulse. In this scheme, switching occurs without a requirement of an external assist field, within the subnanosecond range, and through only a half-rotation ($N = 1/2$) around $\hat{\boldsymbol{\sigma}}$ because the Slonczewski torque prevents **m** from switching back.

In addition, this switching process is not sensitive to the length of the current pulse. As the magnetization directly stabilizes along the switched equilibrium direction under the application of currents [see Fig. 1(d)], any pulse length longer than the switching time is able to deterministically switch the magnetic layer. Thus, contrary to the OST switching scheme [34,35] and field-pulse-induced magnetic switching [37,39], our proposed scheme does not require precise control of the pulse length. Moreover, we change α from 0.001 to 0.2 in the simulations and find that this half-precession switching mode can be effective for any values of α, because the necessary damping is obtained and adjusted from the Slonczewski torque. However, a high α is still beneficial, as it helps **m** to reach the $-\hat{\mathbf{z}}$ direction faster after the pulse falling edge. A last notable point is that, in this scheme, the two equilibrium directions are conserved at all times, and are equivalent for any current polarity. Both $\hat{\mathbf{z}}$ to $-\hat{\mathbf{z}}$ and $-\hat{\mathbf{z}}$ to $\hat{\mathbf{z}}$ toggle switching can be deterministically achieved regardless of the polarity of the current pulse, in contrast to the quasistatic Slonczewski-torque-induced regime as in Fig. 1(b).

B. Torque dependence

We now extend our study to a large range of the values of $c^{\parallel}/c^{\perp}$ and applied current. Figure 3(a) shows the switching behavior depending on the magnitude of the different torques, with all other parameters being kept identical to those in Fig. 1(d). The pulse is 20 ns long and has infinitely short rising and falling times. The horizontal axis and vertical axis correspond to the strengths of the fieldlike ($h^{\perp}$) and the Slonczewski ($h^{\parallel}$) torques, respectively. Blue denotes the regions where magnetization switching is achieved, while red denotes the regions where the magnetization remains in its initial state. For the low positive values of the torque ratio ($c^{\parallel}/c^{\perp} < \sim0.01$), the damping of the trajectory arising from the Slonczewski torque remains low. Then many precessions around $\hat{\boldsymbol{\sigma}}$ occur, and switching is nondeterministic as the final position after 20 ns is still not stabilized and cannot be predicted. This corresponds to the mixed blue and red horizontal stripe in Fig. 3(a). However, when both torques are of same sign with a
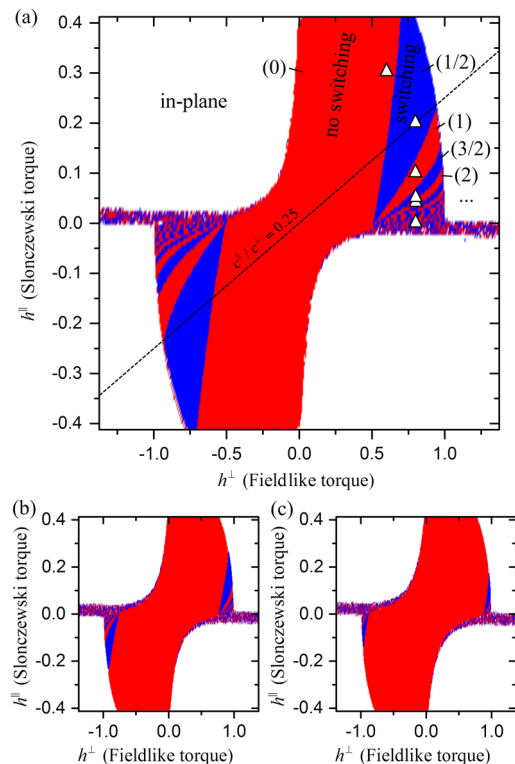

FIG. 3. Final position at the end of the pulse as a function of the strengths of the Slonczewski and fieldlike torques with $t_{\text{rise}} = 0$ (a), $t_{\text{rise}} = 300$ ps (b), and $t_{\text{rise}} = 1000$ ps (c). Red regions indicate unswitched regimes, blue represents switched regimes, and white domains denote when **m** lies in-plane. In (a), the dashed line shows the torques that correspond to $c^{\parallel}/c^{\perp} = 0.25$. Triangles indicate the different cases shown in Fig. 1(d) and Fig. 2. Numbers in brackets are the precession number *N*.

significant Slonczewski torque ($c^{\parallel}/c^{\perp} > \sim0.01$), the precession number *N* can be determined as **m** reaches a final, stable position before the falling edge of the pulse, and deterministic switching (or nonswitching) is observed.

Depending on *N*, **m** switches via half-precession ($N = 1/2$), switches via more than one precession ($N = 3/2, 5/2, \ldots$), does not switch after some precessions ($N = 1, 2, \ldots$), or does not attempt switching at all ($N = 0$). The particular values of the torques $h^{\perp}$ and $h^{\parallel}$ in Fig. 1(d) and Figs. 2(b)–2(f) are marked by the white triangles in Fig. 3(a). When the torque resulting from the combination of $h^{\perp}$ and $h^{\parallel}$ is too strong, the up and down equilibria merge with the equilibrium located at $\hat{\boldsymbol{\sigma}}$, and the stable **m** under the application of currents lies in-plane along $\hat{\boldsymbol{\sigma}}$. Due to the symmetry of the system, the subsequent relaxation is nondeterministic with equal probabilities of relaxation either along $+\hat{\mathbf{z}}$ or $-\hat{\mathbf{z}}$ (considering thermal fluctuations). The white domains in Fig. 3(a) correspond to **m** in-plane under the application of currents. In the absence of Slonczewski torque, the condition for up and down merging is derived as $h^{\perp} \geq 1$.

Among these outcomes, the most interesting case is switching via half-precession. This case corresponds to the

blue regions labeled (1/2) in Fig. 3(a). This region extends to a significant range of the diagram, therefore switching via half-precession is quite robust with respect to the relative values of $c^{\parallel}$ and $c^{\perp}$. Moreover, for some values of $c^{\parallel}/c^{\perp}$, we observe that N is limited to 0 or 1/2. The case of $c^{\parallel}/c^{\perp} = 0.25$, for example, is shown by the dashed line in Fig. 3(a). We can further compare this scheme with field-induced switching using pulses of undefined length, for which the suitable current intensity is strongly linked to α [37]. Because α is fixed by the material choice in a device, the window of the switching field amplitudes is limited. In our situation, on the contrary, where the damping arises from the Slonczewski torque, the effective damping is proportional to the current. For greater switching currents, that is, greater initial lags, the effective damping is also stronger and balances the lag so that switching can still be achieved by half-precession.

Having $N \leq 1/2$ on the whole range of current densities allows a reliable switching behavior regardless of the variations of the amplitude of the current. The required range of $c^{\parallel}/c^{\perp}$ to observe this regime without switching back is found to be 0.23–0.55, with $\alpha = 0.01$. Interestingly, among the several material combinations studied so far, the ratio $c^{\parallel}/c^{\perp}$ of Ta/CoFeB/MgO has been reported to be in this range [24,26,27] as well as that of Hf/CoFeB/MgO [28]. It is noteworthy that if the signs of $c^{\parallel}$ and $c^{\perp}$ are not same ($c^{\parallel}/c^{\perp} < 0$), reliable switching is not observed or the magnetization stabilizes in the *x*-*y* plane, as indicated by the white area in the second and fourth quadrants in Fig. 3(a). Note that the switching characteristics are not noticeably modified for values of $t_{\text{rise}} \leq 50$ ps, but are altered for larger t_{rise} values, as can be seen from Figs. 3(b) and 3(c), corresponding to $t_{\text{rise}} = 300$ ps and $t_{\text{rise}} = 1000$ ps, respectively. We thus need to consider the influence of the rising time on switching.

C. Influence of rising time

So far we have discussed the fieldlike-torque-dominated switching by modeling the current pulse with $t_{\text{rise}} = 0$. This is an ideal case, and switching strongly relies on the initial lag of the magnetization. In the case of a finite rising time, the switching behavior can be altered. Figure 4(a) shows the switching trajectories with $h^{\parallel} = 0.2$ and $h^{\perp} = 0.8$, with different values of t_{rise}. For the shorter rising times (blue and green lines corresponding to $t_{\text{rise}} = 50$ ps and 200 ps, or $t'_{\text{rise}} \approx 0.3\pi$ and 1.2π, respectively), the magnetization reverses by half-precession, as expected. For $t_{\text{rise}} = 50$ ps, the trajectory is not noticeably changed with respect to the case of an infinitely sharp pulse, but the point where **m** crosses the *xy* plane is displaced towards the saddle point located in the direction of $\hat{\boldsymbol{\sigma}}$ when t_{rise} further increases to $t_{\text{rise}} = 200$ ps. For the longer t_{rise} (orange and red lines corresponding to $t_{\text{rise}} = 400$ ps and 800 ps, or $t'_{\text{rise}} \approx 2.2\pi$ and 4.5π, respectively), **m** evolves significantly and the
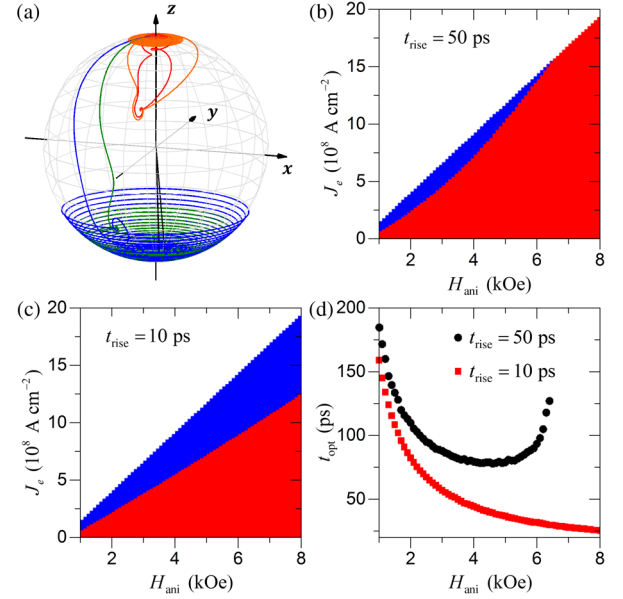

FIG. 4.   (a) Switching trajectories for different t_{rise} (blue is 50 ps, green is 200 ps, orange is 400 ps, and red is 800 ps) with $h^{\parallel} = 0.2$ and $h^{\perp} = 0.8$. Switching behavior depending on H_{ani} and J_e for $t_{\text{rise}} = 50$ ps (b) and $t_{\text{rise}} = 10$ ps (c). Red regions indicate unswitched and blue represents switched regimes, while white denotes current densities for which **m** lies in-plane during the pulse. (d) Optimal switching time (t_{opt}) versus anisotropy for the two t_{rise} values. For (b)–(d), $c^{\parallel} = 0.07$ and $c^{\perp} = 0.28$.

additional energy is dissipated during the rising edge of the pulse. This reduces the initial amplitude of the trajectory so that **m** does not reach the *x*-*y* plane and cannot switch. As a consequence, for the same pulse amplitude, the longer rising times lead to less efficient switching or even prevent switching.

D. Switching times

We now discuss the achievable switching times. According to the last term of Eq. (4), the frequency of the current-induced precession around $\hat{\boldsymbol{\sigma}}$ is roughly proportional to the fieldlike-torque term, and thus the switching speed is also expected to be proportional to the current density J_e. However, we saw earlier that, once the SOT effective field overcomes the anisotropy field, **m** aligns with $\hat{\boldsymbol{\sigma}}$ and switching is subject to a stochastic behavior. It is, thus, not possible to increase J_e arbitrarily in order to induce faster precession around $\hat{\boldsymbol{\sigma}}$ and reduce the switching time. Therefore, other means are required to reduce the switching time. When varying H_{ani}, only the scale factor between t and t' as well as J_0 are modified. As a consequence, multiplying both H_{ani} and J_e by a common factor, Eq. (4) and all parameters remain unchanged so that the switching trajectory is identical, with faster switching. For the switching to be exactly reproduced, any rising time of the pulse should also be reduced accordingly. However,

$t_{\rm rise}$ is actually an experimental and practical limitation that is fixed. Increasing $H_{\rm ani}$ up to $t'_{\rm rise} \approx 2\pi$, the initial lag is altered and switching is no longer achievable as discussed earlier. Nevertheless, in the range of anisotropies that allow switching for a given $t_{\rm rise}$, one can increase $H_{\rm ani}$ to achieve faster, almost identical switching at a higher J_e.

Figures 4(b) and 4(c) compare the range of suitable switching current densities for $H_{\rm ani} = 1$–8 kOe, with $t_{\rm rise} = 50$ ps and 10 ps, respectively. With the torque efficiencies $c^{\parallel} = 0.07$ and $c^{\perp} = 0.28$ ($c^{\parallel}/c^{\perp} = 0.25$) chosen in accord with experimental findings [24,26,27], a current density $J_e = 2.1 \times 10^8$ A cm^{-2} at $H_{\rm ani} = 1$ kOe corresponds to the values $h^{\parallel} = 0.2$ and $h^{\perp} = 0.8$, previously considered in Figs. 1(d) and 4(a). It is experimentally feasible to achieve $t_{\rm rise} = 50$ ps [40], which would require state-of-the-art electronics and a well-calibrated device design, while $t_{\rm rise} = 10$ ps is close to an ideal case. At $H_{\rm ani} = 1$ kOe, $t_{\rm rise} = 50$ ps and 10 ps correspond to $t'_{\rm rise} \approx 0.28\pi$ and 0.06π, respectively, while at $H_{\rm ani} = 8$ kOe, they correspond to $t'_{\rm rise} \approx 2.25\pi$ and 0.45π, respectively. As in Fig. 3, red in Figs. 4(b) and 4(c) corresponds to an unswitched final state, blue indicates proper switching, and white denotes when the current density is too high for the anisotropy and drives **m** in-plane. It is clear in Fig. 4(b) that the critical current density for switching is proportional to $H_{\rm ani}$ up to $H_{\rm ani} = 6.5$ kOe, beyond which switching cannot be achieved because $t'_{\rm rise} \approx 2\pi$.

When $t_{\rm rise}$ is shortened from 50 to 10 ps, a clear switching window whose limits are proportional to $H_{\rm ani}$ is obtained even for the higher anisotropies as $t'_{\rm rise} \ll 2\pi$. As Figs. 4(b) and 4(c) are modified by the finite rising time of the pulse, one can also understand the role of $t_{\rm rise}$ in Fig. 3. Increasing $t_{\rm rise}$ decreases the initial lag of **m** and the initial energy shift, so that the energy provided by the fieldlike torque should be increased and the energy dissipation by the Slonczewski torque should be reduced accordingly, in order to succeed to switch **m**. That lower efficiency causes the different switching domains in Fig. 3(a) to shrink. All the different domains with $N \geq 1/2$ are greatly reduced with $t_{\rm rise} = 300$ ps ($t'_{\rm rise} \approx 1.7\pi$), as can be seen in Fig. 3(b). They are even almost suppressed for $t_{\rm rise} \geq 1000$ ps ($t'_{\rm rise} \geq 5.5\pi$), and the central part is entirely occupied by the nonswitching red domain $N = 0$ [Fig. 3(c)], as expected in the almost quasistatic regime.

As mentioned earlier, increasing the anisotropy constant aims at reducing the switching times. Figure 5(a) shows, for example, the time evolution of **m** with $H_{\rm ani} = 1$ kOe, $J_e = 2.1 \times 10^8$ A cm^{-2}, and $t_{\rm rise} = 50$ ps. The switching time $t_{\rm sw}$ is defined as the time difference between the start of the rising edge of the current pulse and the time when **m** crosses the x-y plane, as represented in Fig. 5(a). As shown in Fig. 5(b), increasing both $H_{\rm ani}$ and J_e threefold causes $t_{\rm sw}$ to decrease from 170 to 90 ps, following a similar trajectory. However, $t_{\rm sw}$ is not shortened by a factor of 3 because of the fixed value of $t_{\rm rise} = 50$ ps.
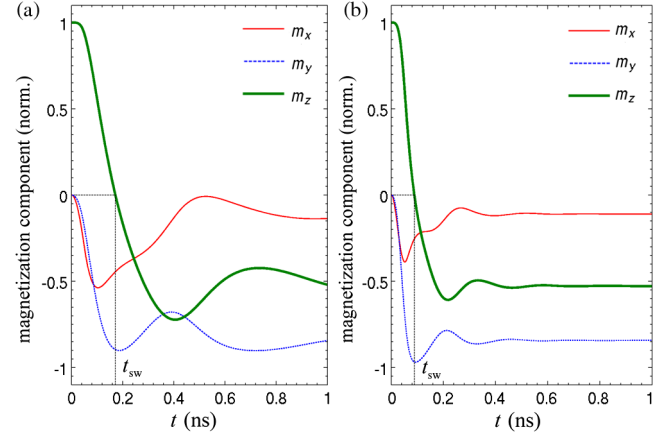

FIG. 5. Time evolution of **m** with $t_{\rm rise} = 50$ ps, $c^{\parallel} = 0.07$, and $c^{\perp} = 0.28$ for (a) $H_{\rm ani} = 1$ kOe and $J_e = 2.1 \times 10^8$ A cm^{-2}, and (b) $H_{\rm ani} = 3$ kOe and $J_e = 6.3 \times 10^8$ A cm^{-2}.

We can relate the evolution of the window shown in Fig. 4(b) and the evolution of $t_{\rm sw}$. Within the range of current densities that enables switching at a given $H_{\rm ani}$, the value of $t_{\rm sw}$ can slightly vary. For the purpose of comparison between the different anisotropies, we define at each value of $H_{\rm ani}$ the optimal switching time $t_{\rm opt}$ as the value of $t_{\rm sw}$ obtained for the central J_e in the range of properly switching currents. Figure 4(d) shows $t_{\rm opt}$ as a function of $H_{\rm ani}$, for both $t_{\rm rise} = 50$ and 10 ps. The smallest switching time with $t_{\rm rise} = 50$ ps is $t_{\rm opt} \approx 80$ ps, obtained near $H_{\rm ani} = 4$ kOe and $J_e = 8.4 \times 10^8$ A cm^{-2}. With $t_{\rm rise} = 10$ ps, a shorter switching time ($t_{\rm opt} \approx 25$ ps and less) can be obtained by increasing $H_{\rm ani}$ to 8 kOe and more. As expected, $t_{\rm opt}$ is initially inversely proportional to $H_{\rm ani}$ as $t'_{\rm rise} \ll 2\pi$, as can be seen from the black curve ($H_{\rm ani} = 1$–3 kOe) or from the red curve in Fig. 4(d). Then $t_{\rm opt}$ with $t_{\rm rise} = 50$ ps reaches a minimum value before it increases with the anisotropy. This trend corresponds to the narrowing of the window of switching currents that can be seen in Fig. 4(b). The switching time $t_{\rm opt}$ increases more and more rapidly as $H_{\rm ani}$ reaches the limit value for which $t'_{\rm rise} \approx 2\pi$, beyond which no switching is observed. For a particular value of $t_{\rm rise}$, J_e and $H_{\rm ani}$ can be tuned for the smallest $t_{\rm opt}$. As long as $t_{\rm rise}$ is much shorter than $t_{\rm opt}$, the switching time evolves as $1/H_{\rm ani}$ while the required J_e is proportional to $H_{\rm ani}$, so that increasing the anisotropy to achieve faster switching does not require more energy to be dissipated in the device.

IV. MICROMAGNETIC SIMULATIONS

We finally discuss the validity of the macrospin model regarding the size of the device, as the macrospin behavior is an essential assumption in the study presented above. We perform micromagnetic simulations of SOT switching without assist field. We now include the nonuniform magnetization contribution that can be expressed as

$$E_{\mathrm{nu}} = A_{\mathrm{ex}}\left[\left(\frac{\partial \mathbf{m}}{\partial x}\right)^2 + \left(\frac{\partial \mathbf{m}}{\partial y}\right)^2\right]$$
$$+ D\left(m_z\frac{\partial m_x}{\partial x} - m_x\frac{\partial m_z}{\partial x} + m_z\frac{\partial m_y}{\partial y} - m_y\frac{\partial m_z}{\partial y}\right), \quad (5)$$

where the first term is the exchange energy density (A_{ex} is the exchange constant) and the second term is the DMI energy density (D is the DMI parameter). The total energy density is then given at each point of the ferromagnet by

$$E_{\mathrm{tot}} = K_u[1 - (\mathbf{m}\cdot\hat{\mathbf{z}})^2] - \frac{1}{2}\mu_0 M_S\mathbf{H}_{\mathbf{demag}}\cdot\mathbf{m} + E_{\mathrm{nu}}, \quad (6)$$

where K_u is the perpendicular uniaxial anisotropy and $\mathbf{H}_{\mathbf{demag}}$ is the magnetostatic demagnetizing field. From Eqs. (5) and (6), it appears that the DMI can stabilize a nonuniform magnetization inside the nanomagnet, opposing the exchange coupling. In order to compare with the results of the above macrospin study, the same simulation parameters are used with an exchange stiffness $A_{\mathrm{ex}} = 3 \times 10^{-11}$ J m^{-1} [41]. Among various materials, the DMI constant is experimentally determined as $|D| \approx 0.053$ mJ m^{-2} for Ta/CoFe/MgO and $|D| \approx 1.2$ mJ m^{-2} for Pt/CoFe/MgO [42], while $|D| \approx 1.0$ mJ m^{-2} for Pt/CoFeB/MgO [43]. For Hf or W/CoFeB/MgO, different thickness-dependent values up to $|D| \approx 0.5$ mJ m^{-2} have been reported [44]. We therefore consider either no DMI ($D = 0$) or an intermediate DMI strength ($D = 0.5$ mJ m^{-2}) for this study.

When the DMI is absent ($D = 0$) and for a device size of $50 \times 50 \times 1.6$ nm^3 (cell size of $2.5 \times 2.5 \times 0.8$ nm^3), we clearly observe a reversal of the magnetization through uniform motion, in particular when no assist field is applied. Increasing $c^{\parallel}/c^{\perp}$ from 0 to 0.5, we find various switching regimes such as a nondeterministic regime with many successive switchings and switching back, half-precession deterministic switching, and no switching, consistent with the results in Fig. 3(a). We also observe that the higher current densities drive the magnetization in-plane.

We further study the switching behavior of larger samples to understand why switching without an assist field is not observed in the experiments conducted so far. Most previous studies used large patterned samples ($>200 \times 200$ nm^2), in which the DMI may also play a role [20]. We simulate switching for a wide range of current densities, in square nanomagnets with the size $w = 50, 100,$ and 200 nm. As can be seen from Eq. (6), the magnetostatic field $\mathbf{H}_{\mathbf{demag}}$ can compete with the anisotropy, reducing the strength of the effective anisotropy field H_{ani}. In order to get switching currents comparable with the previous macrospin study for each size, we compensate the increasing demagnetization energy term with w by increasing the uniaxial magnetic anisotropy energy K_u as well, so that the effective anisotropy

remains $H_{\mathrm{ani}} = 1000$ Oe for all sizes. During the relaxation phase after the pulse, the damping parameter is set to $\alpha = 0.3$ for faster convergence. Note that because of the different demagnetizing fields in the center and in the corners, the switching behavior is no longer ideal. In particular, $c^{\parallel}/c^{\perp} = 0.3$ is used to avoid switching back from the edges in some cases.

Figures 6(a)–6(f) show the mean value of the m_z component at the end of the current pulse (green circles) and after relaxation (red stars) as a function of J_e for various w sizes and DMI parameters. The inset of each figure is a map (top view) of the m_z component in the ferromagnet, just before the falling edge of the pulse for a current density of 1.43×10^8 A cm^{-2}, with the corresponding point indicated by an arrow in each figure. Red, white, and blue regions correspond to the m_z values indicated by the color bar in Fig. 6(d). Without DMI [Figs. 6(a)–6(c)], the switching process leads to a uniform state that relaxes to $\mathbf{m} = -\hat{\mathbf{z}}$ after the pulse. As can be inferred from the large white area in the inset of Fig. 6(c), the magnetostatic energies become more important with increasing device sizes, leading to nonuniform magnetization and noncoherent motion in the larger devices. This alters the switching process as the macrospin behavior is no longer valid, and significantly reduces the window of effective switching currents. With $w = 200$ nm, switching is observed only for high current densities that drive $\mathbf{m}$ almost in-plane, where thermal fluctuations may disrupt reliable switching. As a consequence, deterministic switching without an assist field is not expected in larger nanomagnets.

Furthermore, the detrimental influence of w on switching is reinforced by the contribution of the DMI. The DMI leads to domain-wall formation and nonuniformity of the magnetization within the ferromagnetic layer. In the case of $w = 50$ nm with $D = 0.5$ mJ m^{-2}, coherent switching through quasiuniform motion of $\mathbf{m}$ [whose state at the end of the pulse is represented in the inset labeled (i) in Fig. 6(d)] can occur only for limited current densities. For higher current densities, as $\mathbf{m}$ is closer to the x-y plane, the DMI overcomes the exchange interaction and leads to a multidomain final state that can be seen from the inset labeled (ii) in Fig. 6(d). In the cases of $w = 100$ nm and $w = 200$ nm [Figs. 6(e) and 6(f), respectively], the DMI disrupts the uniform motion of $\mathbf{m}$ and no switching is achieved. Therefore, switching in the absence of an external assist field is expected only in small devices where the DMI is weak, for example, using Ta for the HM layer. The influence of the DMI may be reduced, when H_{ani} is much higher. However, the higher the anisotropy is, the shorter the rise time t_{rise} has to be. When the effective perpendicular anisotropy is of the order of 4 kOe or more, in most experiments conducted so far (e.g., Ref. [19]), t_{rise} should be ~ 50 ps or less. In addition to the detrimental influences of w and D, larger rising times in experiments
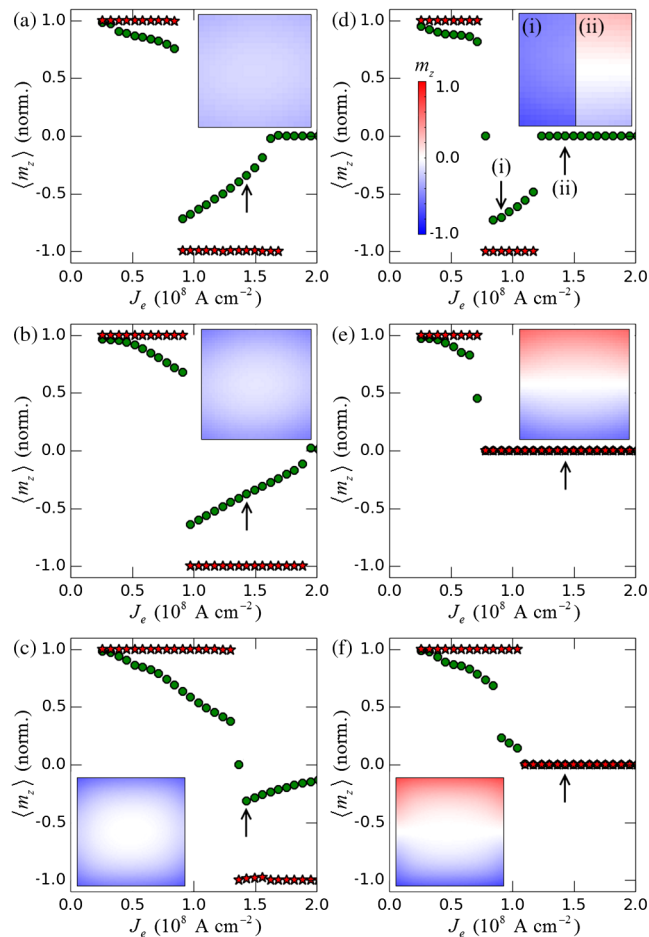
FIG. 6. Mean value of the m_z component of **m** at the end of the current pulse (green circles) and after relaxation (red stars) depending on J_e for (a) $w = 50$ nm and $D = 0$, (b) $w = 100$ nm and $D = 0$, (c) $w = 200$ nm and $D = 0$, (d) $w = 50$ nm and $D = 0.5$ mJ m^{-2}, (e) $w = 100$ nm and $D = 0.5$ mJ m^{-2}, and (f) $w = 200$ nm and $D = 0.5$ mJ m^{-2}. The inset of each figure is a map of the m_z component in the ferromagnet immediately before the falling edge of the pulse for a current density of 1.43×10^8 A cm^{-2}, with the corresponding point indicated by an arrow in each case. Colors correspond to the m_z values indicated by the color scale in (d). In the particular case of (d), two arrows labeled (i) and (ii) indicate two different situations under current densities of 0.91×10^8 A cm^{-2} and 1.43×10^8 A cm^{-2}, respectively.

will prevent switching, which may explain why coherent switching driven by the fieldlike torque has not been experimentally achieved.

V. SUMMARY

We propose a regime of magnetization switching exploiting the fieldlike spin-orbit torque, so that switching does not require any assist field. When the relative efficiencies of the torques match a required range of ratios (0.23–0.55) between the Slonczewski and the fieldlike torques,

magnetization reversal can occur deterministically through a half-precession trajectory within tens of picoseconds. This regime is found to be insensitive to the length of the applied pulse, thus allowing reliable switching. When the rise time of the current pulse is short enough, a higher-anisotropy ferromagnet allows faster switching for the same pulse energy in the limit of the single-domain behavior. The proposed current-induced SOT switching may be compatible, for example, with the Ta-based trilayer systems. The possibility of achieving reliable current-induced SOT switching without applying external fields paves a way to utilize SOT switching for memory-device applications.

[1] I. M. Miron, G. Gaudin, S. Auffret, B. Rodmacq, A. Schuhl, S. Pizzini, J. Vogel, and P. Gambardella, Current-driven spin torque induced by the Rashba effect in a ferromagnetic metal layer, Nat. Mater. **9**, 230 (2010).

[2] S. Emori, U. Bauer, S.-M. Ahn, E. Martinez, and G. S. D. Beach, Current-driven dynamics of chiral ferromagnetic domain walls, Nat. Mater. **12**, 611 (2013).

[3] K.-S. Ryu, L. Thomas, S.-H. Yang, and S. Parkin, Chiral spin torque at magnetic domain walls, Nat. Nanotechnol. **8**, 527 (2013).

[4] T. Suzuki, S. Fukami, N. Ishiwata, M. Yamanouchi, S. Ikeda, N. Kasai, and H. Ohno, Current-induced effective field in perpendicularly magnetized Ta/CoFeB/MgO wire, Appl. Phys. Lett. **98**, 142505 (2011).

[5] I. M. Miron, K. Garello, G. Gaudin, P.-J. Zermatten, M. V. Costache, S. Auffret, S. Bandiera, B. Rodmacq, A. Schuhl, and P. Gambardella, Perpendicular switching of a single ferromagnetic layer induced by in-plane current injection, Nature (London) **476**, 189 (2011).

[6] L. Liu, C. F. Pai, Y. Li, H. W. Tseng, D. C. Ralph, and R. A. Buhrman, Spin-torque switching with the giant spin hall effect of tantalum, Science **336**, 555 (2012).

[7] L. Liu, O. J. Lee, T. J. Gudmundsen, D. C. Ralph, and R. A. Buhrman, Current-Induced Switching of Perpendicularly Magnetized Magnetic Layers Using Spin Torque from the Spin Hall Effect, Phys. Rev. Lett. **109**, 096602 (2012).

[8] C.-F. Pai, L. Liu, Y. Li, H. W. Tseng, D. C. Ralph, and R. A. Buhrman, Spin transfer torque devices utilizing the giant spin Hall effect of tungsten, Appl. Phys. Lett. **101**, 122404 (2012).

[9] L. Liu, C.-F. Pai, D. C. Ralph, and R. A. Buhrman, Magnetic Oscillations Driven by the Spin Hall Effect in 3-Terminal Magnetic Tunnel Junction Devices, Phys. Rev. Lett. **109**, 186602 (2012).

[10] V. E. Demidov, S. Urazhdin, H. Ulrichs, V. Tiberkevich, A. Slavin, D. Baither, G. Schmitz, and S. O. Demokritov, Magnetic nano-oscillator driven by pure spin current, Nat. Mater. **11**, 1028 (2012).

[11] R. Liu, W. Lim, and S. Urazhdin, Spectral Characteristics of the Microwave Emission by the Spin Hall Nano-Oscillator, Phys. Rev. Lett. **110**, 147601 (2013).

[12] M. Cubukcu, O. Boulle, M. Drouard, K. Garello, C. O. Avci, I. M. Miron, J. Langer, B. Ocker, P. Gambardella, and G. Gaudin, Spin-orbit torque magnetization switching of a three-terminal perpendicular magnetic tunnel junction, Appl. Phys. Lett. **104**, 042406 (2014).

[13] P. P. J. Haazen, E. Murè, J. H. Franken, R. Lavrijsen, H. J. M. Swagten, and B. Koopmans, Domain wall depinning governed by the spin Hall effect, Nat. Mater. **12**, 299 (2013).

[14] A. Manchon and S. Zhang, Theory of spin torque due to spin-orbit coupling, Phys. Rev. B **79**, 094422 (2009).

[15] X. Wang and A. Manchon, Diffusive Spin Dynamics in Ferromagnetic Thin Films with a Rashba Interaction, Phys. Rev. Lett. **108**, 117201 (2012).

[16] M. Jamali, K. Narayanapillai, X. Qiu, L. Loong, A. Manchon, and H. Yang, Spin-Orbit Torques in Co/Pd Multilayer Nanowires, Phys. Rev. Lett. **111**, 246602 (2013).

[17] X. Qiu, K. Narayanapillai, Y. Wu, P. Deorani, D.-H. Yang, W.-S. Noh, J.-H. Park, K.-J. Lee, H.-W. Lee, and H. Yang, Spin-orbit-torque engineering via oxygen manipulation, Nat. Nanotechnol. **10**, 333 (2015).

[18] S. Mangin, D. Ravelosona, J. A. Katine, M. J. Carey, B. D. Terris, and E. E. Fullerton, Current-induced magnetization reversal in nanopillars with perpendicular anisotropy, Nat. Mater. **5**, 210 (2006).

[19] K. Garello, C. O. Avci, I. M. Miron, M. Baumgartner, A. Ghosh, S. Auffret, O. Boulle, G. Gaudin, and P. Gambardella, Ultrafast magnetization switching by spin-orbit torques, Appl. Phys. Lett. **105**, 212402 (2014).

[20] O. J. Lee, L. Q. Liu, C. F. Pai, Y. Li, H. W. Tseng, P. G. Gowtham, J. P. Park, D. C. Ralph, and R. A. Buhrman, Central role of domain wall depinning for perpendicular magnetization switching driven by spin torque from the spin Hall effect, Phys. Rev. B **89**, 024418 (2014).

[21] G. Yu, P. Upadhyaya, Y. Fan, J. G. Alzate, W. Jiang, K. L. Wong, S. Takei, S. A. Bender, L.-T. Chang, Y. Jiang, M. Lang, J. Tang, Y. Wang, Y. Tserkovnyak, P. K. Amiri, and K. L. Wang, Switching of perpendicular magnetization by spin-orbit torques in the absence of external magnetic fields, Nat. Nanotechnol. **9**, 548 (2014).

[22] L. You, O. Lee, D. Bhowmik, D. Labanowski, J. Hong, J. Bokor, and S. Salahuddin, Switching of perpendicularly polarized nanomagnets with spin orbit torque without an external magnetic field by engineering a tilted anisotropy, arXiv:1409.0620.

[23] K.-W. Kim, S.-M. Seo, J. Ryu, K.-J. Lee, and H.-W. Lee, Magnetization dynamics induced by in-plane currents in ultrathin magnetic nanostructures with Rashba spin-orbit coupling, Phys. Rev. B **85**, 180404 (2012).

[24] J. Kim, J. Sinha, M. Hayashi, M. Yamanouchi, S. Fukami, T. Suzuki, S. Mitani, and H. Ohno, Layer thickness dependence of the current-induced effective field vector in Ta|CoFeB|MgO, Nat. Mater. **12**, 240 (2013).

[25] K. Garello, I. M. Miron, C. O. Avci, F. Freimuth, Y. Mokrousov, S. Blügel, S. Auffret, O. Boulle, G. Gaudin, and P. Gambardella, Symmetry and magnitude of spin-orbit torques in ferromagnetic heterostructures, Nat. Nanotechnol. **8**, 587 (2013).

[26] C. O. Avci, K. Garello, C. Nistor, S. Godey, B. Ballesteros, A. Mugarza, A. Barla, M. Valvidares, E. Pellegrin, A. Ghosh, I. M. Miron, O. Boulle, S. Auffret, G. Gaudin, and P. Gambardella, Fieldlike and antidamping spin-orbit torques in as-grown and annealed Ta|CoFeB|MgO layers, Phys. Rev. B **89**, 214419 (2014).

[27] X. Qiu, P. Deorani, K. Narayanapillai, K.-S. Lee, K.-J. Lee, H.-W. Lee, and H. Yang, Angular and temperature dependence of current induced spin-orbit effective fields in Ta|CoFeB|MgO nanowires, Sci. Rep. **4**, 4491 (2014).

[28] M. Akyol, J. G. Alzate, G. Yu, P. Upadhyaya, K. L. Wong, A. Ekicibil, P. K. Amiri, and K. L. Wang, Effect of the oxide layer on current-induced spin-orbit torques in Hf|CoFeB|MgO and Hf|CoFeB|TaOx structures, Appl. Phys. Lett. **106**, 032406 (2015).

[29] D. Wang, Spin-orbit field switching of magnetization in ferromagnetic films with perpendicular anisotropy, Appl. Phys. Lett. **100**, 212405 (2012).

[30] L. Liu, T. Moriyama, D. C. Ralph, and R. A. Buhrman, Spin-Torque Ferromagnetic Resonance Induced by the Spin Hall Effect, Phys. Rev. Lett. **106**, 036601 (2011).

[31] K.-S. Lee, S.-W. Lee, B.-C. Min, and K.-J. Lee, Threshold current for switching of a perpendicular magnetic layer induced by spin Hall effect, Appl. Phys. Lett. **102**, 112410 (2013).

[32] K.-S. Lee, S.-W. Lee, B.-C. Min, and K.-J. Lee, Thermally activated switching of perpendicular magnet by spin-orbit spin torque, Appl. Phys. Lett. **104**, 072413 (2014).

[33] J. Park, G. E. Rowlands, O. J. Lee, D. C. Ralph, and R. A. Buhrman, Macrospin modeling of sub-ns pulse switching of perpendicularly magnetized free layer via spin-orbit torques for cryogenic memory applications, Appl. Phys. Lett. **105**, 102404 (2014).

[34] C. Papusoi, B. Delaët, B. Rodmacq, D. Houssameddine, J. P. Michel, U. Ebels, R. C. Sousa, L. Buda-Prejbeanu, and B. Dieny, 100 ps precessional spin-transfer switching of a planar magnetic random access memory cell with perpendicular spin polarizer, Appl. Phys. Lett. **95**, 072506 (2009).

[35] M. Marins de Castro, R. C. Sousa, S. Bandiera, C. Ducruet, A. Chavent, S. Auffret, C. Papusoi, I. L. Prejbeanu, C. Portemont, L. Vila, U. Ebels, B. Rodmacq, and B. Dieny, Precessional spin-transfer switching in a magnetic tunnel junction with a synthetic antiferromagnetic perpendicular polarizer, J. Appl. Phys. **111**, 07C912 (2012).

[36] S. Yan and Y. B. Bazaliy, Phase diagram and optimal switching induced by spin Hall effect in a perpendicular magnetic layer, arXiv:1501.07787.

[37] H. W. Schumacher, C. Chappert, P. Crozat, R. C. Sousa, P. P. Freitas, J. Miltat, J. Fassbender, and B. Hillebrands, Phase Coherent Precessional Magnetization Reversal in Microscopic Spin Valve Elements, Phys. Rev. Lett. **90**, 017201 (2003).

[38] I. Sodemann and Y. B. Bazaliy, Two scenarios of spin-transfer switching and criteria for the corresponding threshold currents, Phys. Rev. B **84**, 064422 (2011).

[39] Y. Shiota, T. Nozaki, F. Bonell, S. Murakami, T. Shinjo, and Y. Suzuki, Induction of coherent magnetization switching in a few atomic layers of FeCo using voltage pulses, Nat. Mater. **11**, 39 (2012).

[40] O. J. Lee, D. C. Ralph, and R. A. Buhrman, Spin-torque-driven ballistic precessional switching with 50 ps impulses, Appl. Phys. Lett. **99**, 102507 (2011).

[41] M. Yamanouchi, A. Jander, P. Dhagat, S. Ikeda, F. Matsukura, and H. Ohno, Domain structure in CoFeB thin films with perpendicular magnetic anisotropy, IEEE Magn. Lett. **2**, 3000304 (2011).

[42] S. Emori, E. Martinez, K.-J. Lee, H.-W. Lee, U. Bauer, S.-M. Ahn, P. Agrawal, D. C. Bono, and G. S. D. Beach, Spin Hall torque magnetometry of Dzyaloshinskii domain walls, Phys. Rev. B **90**, 184427 (2014).

[43] K. Di, V. L. Zhang, H. S. Lim, S. C. Ng, M. H. Kuok, X. Qiu, and H. Yang, Asymmetric spin-wave dispersion due to Dzyaloshinskii-Moriya interaction in an ultrathin Pt/CoFeB film, Appl. Phys. Lett. **106**, 052403 (2015).

[44] J. Torrejon, J. Kim, J. Sinha, S. Mitani, M. Hayashi, M. Yamanouchi, and H. Ohno, Interface control of the magnetic chirality in CoFeB/MgO heterostructures with heavy-metal underlayers, Nat. Commun. **5**, 4655 (2014).